

Applications of Nonlinear Fiber Optics

SECOND EDITION



Govind P. Agrawal

Applications of Nonlinear Fiber Optics

Second Edition

This page intentionally left blank

Applications of Nonlinear Fiber Optics

Second Edition

GOVIND P. AGRAWAL

*The Institute of Optics
University of Rochester
Rochester, New York*



ELSEVIER

AMSTERDAM BOSTON HEIDELBERG LONDON
NEW YORK OXFORD PARIS SAN DIEGO
SAN FRANCISCO SINGAPORE SYDNEY TOKYO

Academic Press is an imprint of Elsevier



**ACADEMIC
PRESS**

Academic Press is an imprint of Elsevier
30 Corporate Drive, Suite 400, Burlington, MA 01803, USA
525 B Street, Suite 1900, San Diego, California 92101-4495, USA
84 Theobald's Road, London WC1X 8RR, UK

This book is printed on acid-free paper. ☺

Copyright © 2008 Elsevier Inc. All rights reserved.

No part of this publication may be reproduced or transmitted in any form or by any means, electronic or mechanical, including photocopy, recording, or any information storage and retrieval system, without permission in writing from the publisher.

Requests for permission to make copies of any part of the work should be mailed to: Permissions Department, Harcourt, Inc., 6277 Sea Harbor Drive, Orlando, Florida 32887-6777.

Permissions may be sought directly from Elsevier's Science & Technology Rights Department in Oxford, UK: phone: (+44) 1865 843830, fax: (+44) 1865 853333, E-mail: permissions@elsevier.com. You may also complete your request on-line via the Elsevier homepage (<http://elsevier.com>), by selecting "Support & Contact" then "Copyright and Permission" and then "Obtaining Permissions."

Library of Congress Cataloging-in-Publication Data

Application submitted.

British Library Cataloging-in-Publication Data

A catalogue record for this book is available from the British Library.

ISBN 13: 978-0-12-369516-1

ISBN 10: 0-12-369516-3

For information on all Academic Press publications
visit our Web site at www.books.elsevier.com

Printed in the United States of America
06 07 08 09 10 9 8 7 6 5 4 3 2 1



*In the memory of my parents and
for Anne, Sipra, Caroline, and Claire*

This page intentionally left blank

Contents

Preface	xiii
1 Fiber Gratings	1
1.1 Basic Concepts	1
1.1.1 Bragg Diffraction	2
1.1.2 Photosensitivity	3
1.2 Fabrication Techniques	4
1.2.1 Single-Beam Internal Technique	4
1.2.2 Dual-Beam Holographic Technique	5
1.2.3 Phase-Mask Technique	7
1.2.4 Point-by-Point Fabrication Technique	8
1.2.5 Technique based on Ultrashort Optical Pulses	9
1.3 Grating Characteristics	10
1.3.1 Coupled-Mode Equations	11
1.3.2 CW Solution in the Linear Case	13
1.3.3 Photonic Bandgap	14
1.3.4 Grating as an Optical Filter	16
1.3.5 Experimental Verification	17
1.4 CW Nonlinear Effects	20
1.4.1 Nonlinear Dispersion Curves	20
1.4.2 Optical Bistability	22
1.5 Modulation Instability	24
1.5.1 Linear Stability Analysis	24
1.5.2 Effective NLS Equation	26
1.5.3 Experimental Results	28
1.6 Nonlinear Pulse Propagation	28
1.6.1 Bragg Solitons	29
1.6.2 Relation to NLS Solitons	30
1.6.3 Formation of Bragg Solitons	31
1.6.4 Nonlinear Switching	33
1.6.5 Effects of Birefringence	37
1.7 Related Periodic Structures	39
1.7.1 Long-Period Gratings	39
1.7.2 Nonuniform Bragg Gratings	40

1.7.3	Transient and Dynamic Fiber Gratings	44
	Problems	47
	References	48
2	Fiber Couplers	54
2.1	Coupler Characteristics	54
2.1.1	Coupled-Mode Equations	55
2.1.2	Low-Power Optical Beams	57
2.1.3	Linear Pulse Switching	60
2.2	Nonlinear Effects	61
2.2.1	Quasi-CW Switching	62
2.2.2	Experimental Results	64
2.2.3	Nonlinear Supermodes	66
2.2.4	Modulation Instability	67
2.3	Ultrashort Pulse Propagation	70
2.3.1	Nonlinear Switching of Optical Pulses	71
2.3.2	Variational Approach	73
2.3.3	Coupler-Paired Solitons	76
2.3.4	Higher-Order Effects	78
2.4	Other Types of Couplers	81
2.4.1	Asymmetric Couplers	81
2.4.2	Active Couplers	83
2.4.3	Grating-Assisted Couplers	85
2.4.4	Birefringent Couplers	87
2.5	Fibers with Multiple Cores	88
2.5.1	Dual-Core Photonic Crystal Fibers	89
2.5.2	Multicore Fiber Arrays	91
	Problems	94
	References	95
3	Fiber Interferometers	100
3.1	Fabry–Perot and Ring Resonators	100
3.1.1	Transmission Resonances	101
3.1.2	Optical Bistability	103
3.1.3	Nonlinear Dynamics and Chaos	105
3.1.4	Modulation Instability	106
3.1.5	Ultrafast Nonlinear Effects	108
3.2	Sagnac Interferometers	110
3.2.1	Nonlinear Transmission	110
3.2.2	Nonlinear Switching	111
3.2.3	Applications	116
3.3	Mach–Zehnder Interferometers	120
3.3.1	Nonlinear Characteristics	120
3.3.2	Applications	123
3.4	Michelson Interferometers	124
	Problems	125

References	126
4 Fiber Amplifiers	131
4.1 Basic Concepts	131
4.1.1 Pumping and Gain Coefficient	132
4.1.2 Amplifier Gain and Bandwidth	133
4.1.3 Amplifier Noise	135
4.2 Erbium-Doped Fiber Amplifiers	136
4.2.1 Gain Spectrum	137
4.2.2 Amplifier Gain	139
4.2.3 Amplifier Noise	142
4.3 Dispersive and Nonlinear Effects	143
4.3.1 Maxwell–Bloch Equations	144
4.3.2 Ginzburg–Landau Equation	145
4.4 Modulation Instability	147
4.4.1 Distributed Amplification	147
4.4.2 Periodic Lumped Amplification	148
4.4.3 Noise Amplification	150
4.5 Optical Solitons	151
4.5.1 Properties of Autosolitons	152
4.5.2 Maxwell–Bloch Solitons	155
4.6 Pulse Amplification	157
4.6.1 Anomalous-Dispersion Regime	157
4.6.2 Normal-Dispersion Regime	159
4.6.3 Higher-Order Effects	164
4.7 Fiber-Optic Raman Amplifiers	168
4.7.1 Pulse Amplification Through Raman Gain	168
4.7.2 Self-Similar Evolution and Similariton Formation	170
Problems	172
References	173
5 Fiber Lasers	179
5.1 Basic Concepts	179
5.1.1 Pumping and Optical Gain	180
5.1.2 Cavity Design	181
5.1.3 Laser Threshold and Output Power	183
5.2 CW Fiber Lasers	185
5.2.1 Nd-Doped Fiber Lasers	185
5.2.2 Yb-Doped Fiber Lasers	187
5.2.3 Erbium-Doped Fiber Lasers	190
5.2.4 DFB Fiber Lasers	192
5.2.5 Self-Pulsing and Chaos	195
5.3 Short-Pulse Fiber Lasers	197
5.3.1 Q-Switched Fiber Lasers	197
5.3.2 Physics of Mode Locking	200
5.3.3 Active Mode Locking	201

5.3.4	Harmonic Mode Locking	205
5.4	Passive Mode Locking	210
5.4.1	Saturable Absorbers	210
5.4.2	Nonlinear Fiber-Loop Mirrors	213
5.4.3	Nonlinear Polarization Rotation	216
5.4.4	Hybrid Mode Locking	219
5.4.5	Other Mode-Locking Techniques	221
5.5	Role of Fiber Nonlinearity and Dispersion	226
5.5.1	Saturable-Absorber Mode Locking	226
5.5.2	Additive-Pulse Mode Locking	227
5.5.3	Spectral Sidebands and Pulse Width	228
5.5.4	Phase Locking and Soliton Collisions	231
5.5.5	Polarization Effects	233
	Problems	235
	References	235
6	Pulse Compression	245
6.1	Physical Mechanism	245
6.2	Grating-Fiber Compressors	247
6.2.1	Grating Pair	248
6.2.2	Optimum Compressor Design	250
6.2.3	Practical Limitations	253
6.2.4	Experimental Results	254
6.3	Soliton-Effect Compressors	259
6.3.1	Compressor Optimization	259
6.3.2	Experimental Results	261
6.3.3	Higher-Order Nonlinear Effects	263
6.4	Fiber Bragg Gratings	266
6.4.1	Gratings as a Compact Dispersive Element	267
6.4.2	Grating-Induced Nonlinear Chirp	268
6.4.3	Bragg-Soliton Compression	270
6.5	Chirped-Pulse Amplification	271
6.5.1	Chirped Fiber Gratings	272
6.5.2	Photonic Crystal Fibers	274
6.6	Dispersion-Managed Fibers	276
6.6.1	Dispersion-Decreasing Fibers	276
6.6.2	Comb-like Dispersion Profiles	281
6.7	Other Compression Techniques	283
6.7.1	Cross-Phase Modulation	283
6.7.2	Gain Switching in Semiconductor Lasers	286
6.7.3	Optical Amplifiers	287
6.7.4	Fiber-Loop Mirrors and Other Devices	290
	Problems	292
	References	293

7	Fiber-Optic Communications	301
7.1	System Basics	301
7.1.1	Loss Management	302
7.1.2	Dispersion Management	304
7.2	Impact of Fiber Nonlinearities	306
7.2.1	Stimulated Brillouin Scattering	306
7.2.2	Stimulated Raman Scattering	308
7.2.3	Self-Phase Modulation	311
7.2.4	Cross-Phase Modulation	315
7.2.5	Four-Wave Mixing	318
7.3	Solitons in Optical Fibers	322
7.3.1	Properties of Optical Solitons	322
7.3.2	Loss-Managed Solitons	325
7.3.3	Dispersion-Managed Solitons	327
7.3.4	Timing Jitter	331
7.4	Pseudo-linear Lightwave Systems	336
7.4.1	Intrachannel Nonlinear Effects	336
7.4.2	Intrachannel XPM	338
7.4.3	Intrachannel FWM	339
	Problems	341
	References	342
8	Optical Signal Processing	349
8.1	Wavelength Conversion	349
8.1.1	XPM-Based Wavelength Converters	350
8.1.2	FWM-Based Wavelength Converters	355
8.2	Ultrafast Optical Switching	360
8.2.1	XPM-Based Sagnac-Loop Switches	360
8.2.2	Polarization-Discriminating Switches	363
8.2.3	FWM-Based Ultrafast Switches	365
8.3	Applications of Time-Domain Switching	368
8.3.1	Channel Demultiplexing	368
8.3.2	Data-Format Conversion	373
8.3.3	All-Optical Sampling	375
8.4	Optical Regenerators	377
8.4.1	SPM-Based Regenerators	377
8.4.2	FWM-Based Regenerators	382
8.4.3	Regeneration of DPSK Signals	384
8.4.4	Optical 3R Regenerators	387
	Problems	390
	References	391

9	Highly Nonlinear Fibers	397
9.1	Microstructured Fibers	397
9.1.1	Design and Fabrication	398
9.1.2	Nonlinear and Dispersive Properties	399
9.2	Wavelength Shifting and Tuning	403
9.2.1	Raman-Induced Frequency shifts	404
9.2.2	Four-Wave Mixing	410
9.3	Supercontinuum Generation	414
9.3.1	Multichannel Telecommunication Sources	415
9.3.2	Nonlinear Spectroscopy	416
9.3.3	Optical Coherence Tomography	420
9.3.4	Optical Frequency Metrology	424
9.4	Photonic Bandgap Fibers	431
9.4.1	Properties of Hollow-Core PCFs	432
9.4.2	Applications of Air-Core PCFs	434
9.4.3	PCFs with Fluid-Filled Cores	436
	Problems	439
	References	440
10	Quantum Applications	447
10.1	Quantum Theory of Pulse Propagation	447
10.1.1	Quantum Nonlinear Schrödinger Equation	448
10.1.2	Quantum Theory of Self-Phase Modulation	449
10.1.3	Generalized NLS Equation	451
10.1.4	Quantum Solitons	452
10.2	Squeezing of Quantum Noise	454
10.2.1	Physics Behind Quadrature Squeezing	454
10.2.2	FWM-Induced Quadrature Squeezing	455
10.2.3	SPM-Induced Quadrature Squeezing	457
10.2.4	SPM-Induced Amplitude Squeezing	461
10.2.5	Polarization Squeezing	466
10.3	Quantum Nondemolition Schemes	468
10.3.1	QND Measurements Through Soliton Collisions	468
10.3.2	QND Measurements Through Spectral Filtering	470
10.4	Quantum Entanglement	472
10.4.1	Photon-Pair Generation	472
10.4.2	Polarization Entanglement	477
10.4.3	Time-Bin Entanglement	481
10.4.4	Continuous-Variable Entanglement	482
10.5	Quantum Cryptography	485
	Problems	487
	References	488
A	Acronyms	493
	Index	495

Preface

Since the publication of the first edition of my book on *Nonlinear Fiber Optics* in 1989, this field has virtually exploded. During the 1990s, a major factor behind such a sustained growth was the advent of fiber amplifiers and lasers, made by doping silica fibers with rare-earth materials such as erbium and ytterbium. Erbium-doped fiber amplifiers revolutionized the design of fiber-optic communication systems, including those making use of optical solitons, whose very existence stems from the presence of nonlinear effects in optical fibers. Optical amplifiers permit propagation of lightwave signals over thousands of kilometers as they can compensate for all losses encountered by the signal in the optical domain. At the same time, fiber amplifiers enable the use of massive wavelength-division multiplexing, a technique that led by 1999 to the development of lightwave systems with capacities exceeding 1 Tb/s. Nonlinear fiber optics plays an important role in the design of such high-capacity lightwave systems. In fact, an understanding of various nonlinear effects occurring inside optical fibers is almost a prerequisite for a lightwave-system designer.

Starting around 2000, a new development occurred in the field of *nonlinear fiber optics* that changed the focus of research and has led to a number of advances and novel applications in recent years. Several kinds of new fibers, classified as highly nonlinear fibers, have been developed. They are referred to with names such as microstructured fibers, holey fibers, or photonic crystal fibers, and share the common property that a relatively narrow core is surrounded by a cladding containing a large number of air holes. The nonlinear effects are enhanced dramatically in such fibers. In fact, with a proper design of microstructured fibers, some nonlinear effects can be observed even when the fiber is only a few centimeters long. The dispersive properties of such fibers are also quite different compared with those of conventional fibers, developed mainly for telecommunication applications. Because of these changes, microstructured fibers exhibit a variety of novel nonlinear effects that are finding applications in the fields as diverse as optical coherence tomography and high-precision frequency metrology.

The fourth edition of *Nonlinear Fiber Optics*, published in 2007, has been updated to include recent developments related to the advent of highly nonlinear fibers. However, it deals mostly with the fundamental aspects of this exciting field. Since 2001, the applications of Nonlinear Fiber Optics have been covered in a companion book that also required updating. This second edition of *Applications of Nonlinear Fiber Optics* fills this need. It has been expanded considerably to include the new research material published over the last seven years or so. It retains most of the material that appeared in the first edition.

The first three chapters deal with three important fiber-optic components—fiber-based gratings, couplers, and interferometers—that serve as the building blocks of lightwave technology. In view of the enormous impact of rare-earth-doped fibers, amplifiers and lasers made by using such fibers are covered in Chapters 4 and 5. Chapter 6 deals with the pulse-compression techniques. Chapters 7 and 8 has been revised extensively to make room for the new material. The former is devoted to fiber-optic communication systems, but Chapter 8 now focuses on the ultrafast signal processing techniques that make use of nonlinear phenomena in optical fibers. Last two chapters, Chapters 9 and 10, are entirely new. Chapter 9 focuses on the applications of highly nonlinear fibers in areas ranging from wavelength laser tuning, nonlinear spectroscopy to biomedical imaging and frequency metrology. Chapter 10 is devoted to the applications of nonlinear fiber optics in the emerging technologies that make use of quantum-mechanical effects. Examples of such technologies include quantum cryptography, quantum computing, and quantum communications.

This volume should serve well the need of the scientific community interested in such diverse fields as ultrafast phenomena, high-power fiber amplifiers and lasers, optical communications, ultrafast signal processing, and quantum information. The potential readership is likely to consist of senior undergraduate students, graduate students enrolled in the M.S. and Ph.D. programs, engineers and technicians involved with the telecommunication and laser industry, and scientists working in the fields of optical communications and quantum information. Some universities may opt to offer a high-level graduate course devoted solely to nonlinear fiber optics. The problems provided at the end of each chapter should be useful to instructors of such a course.

Many individuals have contributed to the completion of this book either directly or indirectly. I am thankful to all of them, especially to my students, whose curiosity led to several improvements. Some of my colleagues have also helped me in preparing this book. I thank Prof. J. H. Eberly, Prof. A. N. Pinto, and Dr. S. Lukishova for reading the chapter on quantum applications and making helpful suggestions. I am grateful to many readers for their feedback. Last, but not least, I thank my wife, Anne, and my daughters, Sipra, Caroline, and Claire, for understanding why I needed to spend many weekends on the book instead of spending time with them.

Govind P. Agrawal

Rochester, NY
December 2007

Chapter 1

Fiber Gratings

Silica fibers can change their optical properties permanently when they are exposed to intense radiation from a laser operating in the blue or ultraviolet spectral region. This photosensitive effect can be used to induce periodic changes in the refractive index along the fiber length, resulting in the formation of an intracore Bragg grating. Fiber gratings can be designed to operate over a wide range of wavelengths extending from the ultraviolet to the infrared region. The wavelength region near $1.5\ \mu\text{m}$ is of particular interest because of its relevance to fiber-optic communication systems. In this chapter on fiber gratings, the emphasis is on the role of the nonlinear effects. Sections 1.1 and 1.2 discuss the physical mechanism responsible for photosensitivity and various techniques used to make fiber gratings. The coupled-mode theory is described in Section 1.3, where the concept of the photonic bandgap is also introduced. Section 1.4 is devoted to the nonlinear effects occurring under continuous-wave (CW) conditions. The phenomenon of modulation instability is then discussed in Section 1.5. The focus of Section 1.6 is on propagation of optical pulses through a fiber grating with emphasis on optical solitons. The phenomenon of nonlinear switching is also covered in this section. Section 1.7 is devoted to related fiber-based periodic structures such as long-period, chirped, sampled, transient, and dynamic gratings together with their applications.

1.1 Basic Concepts

Diffraction gratings constitute a standard optical component and are used routinely in various optical instruments such as a spectrometer. The underlying principle was discovered more than 200 years ago [1]. From a practical standpoint, a diffraction grating is defined as any optical element capable of imposing a periodic variation in the amplitude or phase of light incident on it. Clearly, an optical medium whose refractive index varies periodically acts as a grating since it imposes a periodic variation of phase when light propagates through it. Such gratings are called *index gratings*.

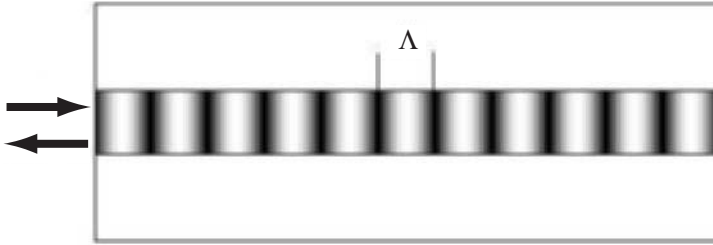


Figure 1.1: Schematic illustration of a fiber grating. Dark and light shaded regions within the fiber core show periodic variations of the refractive index.

1.1.1 Bragg Diffraction

The diffraction theory of gratings shows that when light is incident at an angle θ_i (measured with respect to the planes of constant refractive index), it is diffracted at an angle θ_r such that [1]

$$\sin \theta_i - \sin \theta_r = m\lambda / (\bar{n}\Lambda), \quad (1.1.1)$$

where Λ is the grating period, λ/\bar{n} is the wavelength of light inside the medium with an average refractive index \bar{n} , and m is the order of Bragg diffraction. This condition can be thought of as a phase-matching condition, similar to that occurring in the case of Brillouin scattering or four-wave mixing [2], and can be written as

$$\mathbf{k}_i - \mathbf{k}_d = m\mathbf{k}_g, \quad (1.1.2)$$

where \mathbf{k}_i and \mathbf{k}_d are the wave vectors associated with the incident and diffracted light. The grating wave vector \mathbf{k}_g has magnitude $2\pi/\Lambda$ and points in the direction in which the refractive index of the medium is changing in a periodic manner.

In the case of single-mode fibers, all three vectors lie along the fiber axis. As a result, $\mathbf{k}_d = -\mathbf{k}_i$ and the diffracted light propagates backward. Thus, as shown schematically in Figure 1.1, a fiber grating acts as a reflector for a specific wavelength of light for which the phase-matching condition is satisfied. In terms of the angles appearing in Eq. (1.1.1), $\theta_i = \pi/2$ and $\theta_r = -\pi/2$. If $m = 1$, the period of the grating is related to the vacuum wavelength as $\Lambda = \lambda / (2\bar{n})$. This condition is known as the *Bragg condition*, and gratings satisfying it are referred to as *Bragg gratings*. Physically, the Bragg condition ensures that weak reflections occurring throughout the grating add up in phase to produce a strong reflection at the input end. For a fiber grating reflecting light in the wavelength region near $1.5 \mu\text{m}$, the grating period $\Lambda \approx 0.5 \mu\text{m}$.

Bragg gratings inside optical fibers were first formed in 1978 by irradiating a germanium-doped silica fiber for a few minutes with an intense argon-ion laser beam [3]. The grating period was fixed by the argon-ion laser wavelength, and the grating reflected light only within a narrow region around that wavelength. It was realized that the 4% reflection occurring at the two fiber-air interfaces created a standing-wave pattern such that more of the laser light was absorbed in the bright regions. As a result, the glass structure changed in such a way that the refractive index increased permanently in the bright regions. Although this phenomenon attracted some attention during the next

10 years [4]–[16], it was not until 1989 that fiber gratings became a topic of intense investigation, fueled partly by the observation of second-harmonic generation in photosensitive fibers. The impetus for this resurgence of interest was provided by a 1989 paper in which a side-exposed holographic technique was used to make fiber gratings with controllable period [17].

Because of its relevance to fiber-optic communication systems, the holographic technique was quickly adopted to produce fiber gratings in the wavelength region near $1.55 \mu\text{m}$ [18]. Considerable work was done during the early 1990s to understand the physical mechanism behind photosensitivity of fibers and to develop techniques that were capable of making large changes in the refractive index [19]–[47]. By 1995, fiber gratings were available commercially, and by 1997 they became a standard component of lightwave technology. Soon after, several books devoted entirely to fiber gratings appeared, focusing on applications related to fiber sensors and fiber-optic communication systems [48]–[50].

1.1.2 Photosensitivity

There is considerable evidence that photosensitivity of optical fibers is due to defect formation inside the core of Ge-doped silica (SiO_2) fibers [29]–[31]. In practice, the core of a silica fiber is often doped with germania (GeO_2) to increase its refractive index and introduce an index step at the core-cladding interface. The Ge concentration is typically 3–5% but may exceed 15% in some cases.

The presence of Ge atoms in the fiber core leads to formation of oxygen-deficient bonds (such as Si–Ge, Si–Si, and Ge–Ge bonds), which act as defects in the silica matrix [48]. The most common defect is the GeO defect. It forms a defect band with an energy gap of about 5 eV (energy required to break the bond). Single-photon absorption of 244-nm radiation from an excimer laser (or two-photon absorption of 488-nm light from an argon-ion laser) breaks these defect bonds and creates GeE' centers. Extra electrons associated with GeE' centers are free to move within the glass matrix until they are trapped at hole-defect sites to form the color centers known as Ge(1) and Ge(2). Such modifications in the glass structure change the absorption spectrum $\alpha(\omega)$. However, changes in the absorption also affect the refractive index since $\Delta\alpha$ and Δn are related through the Kramers–Kronig relation [51].

$$\Delta n(\omega') = \frac{c}{\pi} \int_0^\infty \frac{\Delta\alpha(\omega) d\omega}{\omega^2 - \omega'^2}. \quad (1.1.3)$$

Even though absorption modifications occur mainly in the ultraviolet region, the refractive index can change even in the visible or infrared region. Moreover, as index changes occur only in the regions of fiber core where the ultraviolet light is absorbed, a periodic intensity pattern is transformed into an index grating. Typically, index change Δn is 10^{-4} in the 1.3- to 1.6- μm wavelength range, but can exceed 0.001 in fibers with high Ge concentration [34].

The presence of GeO defects is crucial for photosensitivity to occur in optical fibers. However, standard telecommunication fibers rarely have more than 3% of Ge atoms in their core, resulting in relatively small index changes. The use of other dopants such as phosphorus, boron, and aluminum can enhance the photosensitivity (and the amount of

index change) to some extent, but these dopants also tend to increase fiber losses. It was discovered in the early 1990s that the amount of index change induced by ultraviolet absorption can be enhanced by two orders of magnitude ($\Delta n > 0.01$) by soaking the fiber in hydrogen gas at high pressures (200 atm) and room temperature [39]. The density of Ge–Si oxygen-deficient bonds increases in hydrogen-soaked fibers because hydrogen can recombine with oxygen atoms. Once hydrogenated, the fiber needs to be stored at low temperature to maintain its photosensitivity. However, gratings made in such fibers remain intact over relatively long periods of time, if they are stabilized using a suitable annealing technique [52]–[56]. Hydrogen soaking is commonly used for making fiber gratings.

Because of the stability issue associated with hydrogen soaking, a technique, known as ultraviolet (UV) hypersensitization, has been employed in recent years [57]–[59]. An alternative method known as OH flooding is also used for this purpose. In this approach [60], the hydrogen-soaked fiber is heated rapidly to a temperature near 1000 C before it is exposed to UV radiation. The resulting out-gassing of hydrogen creates a flood of OH ions and leads to a considerable increase in the fiber photosensitivity. A comparative study of different techniques revealed that the UV-induced index changes were indeed more stable in the hypersensitized and OH-flooded fibers [61]. It should be stressed that understanding of the exact physical mechanism behind photosensitivity is far from complete, and more than one mechanism may be involved [57]. Localized heating can also affect the formation of a grating. For instance, damage tracks were seen in fibers with a strong grating (index change >0.001) when the grating was examined under an optical microscope [34]; these tracks were due to localized heating to several thousand degrees of the core region where ultraviolet light was most strongly absorbed. At such high temperatures the local structure of amorphous silica can change considerably because of melting.

1.2 Fabrication Techniques

Fiber gratings can be made by using several different techniques, each having its own merits [48]–[50]. This section discusses briefly four major techniques, used commonly for making fiber gratings and known as the single-beam internal technique, the dual-beam holographic technique, the phase-mask technique, and the point-by-point fabrication technique. The use of ultrashort optical pulses for grating fabrication is covered in the last subsection.

1.2.1 Single-Beam Internal Technique

In this technique, used in the original 1978 experiment [3], a single laser beam, often obtained from an argon-ion laser operating in a single mode near 488 nm, is launched into a germanium-doped silica fiber. The light reflected from the near end of the fiber is then monitored. The reflectivity is initially about 4%, as expected for a fiber–air interface. However, it gradually begins to increase with time and can exceed 90% after a few minutes when the Bragg grating is completely formed [5]. Figure 1.2 shows the increase in reflectivity with time, observed in the 1978 experiment for a 1-m-long

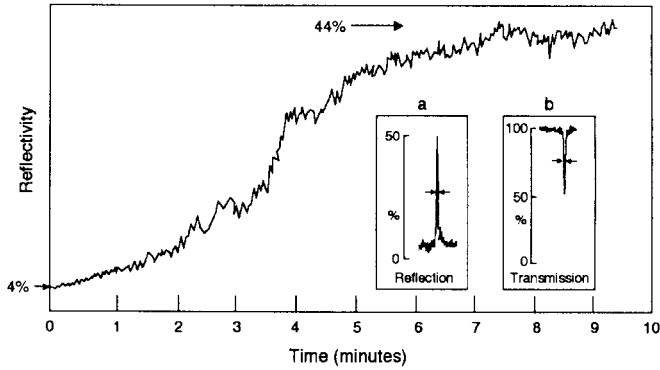


Figure 1.2: Increase in reflectivity with time during grating formation. Insets show the reflection and transmission spectra of the grating. (After Ref. [3]; c 1978 AIP.)

fiber having a numerical aperture of 0.1 and a core diameter of $2.5 \mu\text{m}$. Measured reflectivity of 44% after 8 minutes of exposure implies more than 80% reflectivity of the Bragg grating when coupling losses are accounted for.

Grating formation is initiated by the light reflected from the far end of the fiber and propagating in the backward direction. The two counterpropagating waves interfere and create a standing-wave pattern with periodicity $\lambda/2\bar{n}$, where λ is the laser wavelength and \bar{n} is the mode index at that wavelength. The refractive index of silica is modified locally in the regions of high intensity, resulting in a periodic index variation along the fiber length. Even though the index grating is quite weak initially (4% far-end reflectivity), it reinforces itself through a kind of runaway process. Since the grating period is exactly the same as the standing-wave period, the Bragg condition is satisfied for the laser wavelength. As a result, some forward-traveling light is reflected backward through distributed feedback, which strengthens the grating, which in turn increases feedback. The process stops when the photoinduced index change saturates. Optical fibers with an intracore Bragg grating act as a narrowband reflection filter. The two insets in Figure 1.2 show the measured reflection and transmission spectra of such a fiber grating. The full width at half maximum (FWHM) of these spectra is only about 200 MHz.

A disadvantage of the single-beam internal method is that the grating can be used only near the wavelength of the laser used to make it. Since Ge-doped silica fibers exhibit little photosensitivity at wavelengths longer than $0.5 \mu\text{m}$, such gratings cannot be used in the 1.3- to $1.6\text{-}\mu\text{m}$ wavelength region that is important for optical communications. A dual-beam holographic technique, discussed next, solves this problem.

1.2.2 Dual-Beam Holographic Technique

The dual-beam holographic technique, shown schematically in Figure 1.3, makes use of an external interferometric scheme similar to that used for holography. Two optical beams, obtained from the same laser (operating in the ultraviolet region) and making an angle 2θ are made to interfere at the exposed core of an optical fiber [17]. A cylindrical

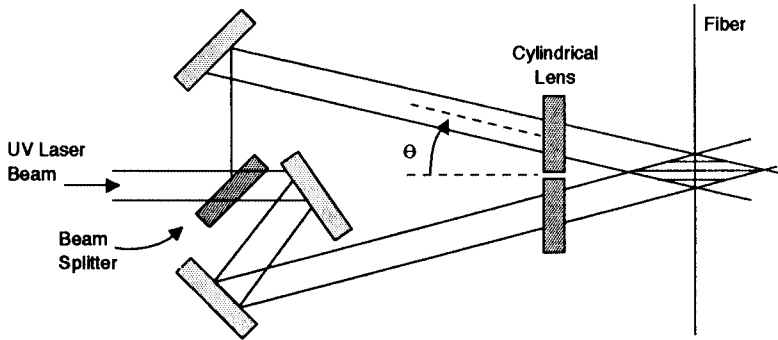


Figure 1.3: Schematic illustration of the dual-beam holographic technique.

lens is used to expand the beam along the fiber length. Similar to the single-beam scheme, the interference pattern creates an index grating. However, the grating period Λ is related to the ultraviolet laser wavelength λ_{uv} and the angle 2θ made by the two interfering beams through the simple relation

$$\Lambda = \lambda_{\text{uv}} / (2 \sin \theta). \quad (1.2.1)$$

The most important feature of the holographic technique is that the grating period Λ can be varied over a wide range by simply adjusting the angle θ (see Figure 1.3). The wavelength λ at which the grating will reflect light is related to Λ as $\lambda = 2n\Lambda$. Since λ can be significantly larger than λ_{uv} , Bragg gratings operating in the visible or infrared region can be fabricated by the dual-beam holographic method even when λ_{uv} is in the ultraviolet region. In a 1989 experiment, Bragg gratings reflecting 580-nm light were made by exposing the 4.4-mm-long core region of a photosensitive fiber for 5 minutes with 244-nm ultraviolet radiation [17]. Reflectivity measurements indicated that the refractive index changes were 10^{-5} in the bright regions of the interference pattern. Bragg gratings formed by the dual-beam holographic technique were stable and remained unchanged even when the fiber was heated to 500 C.

Because of their practical importance, Bragg gratings operating in the 1.55- μm region were made in 1990 [18]. Since then, several variations of the basic technique have been used to make such gratings in a practical manner. An inherent problem for the dual-beam holographic technique is that it requires an ultraviolet laser with excellent temporal and spatial coherence. Excimer lasers commonly used for this purpose have relatively poor beam quality and require special care to maintain the interference pattern over the fiber core over a duration of several minutes.

It turns out that high-reflectivity fiber gratings can be written by using a single excimer laser pulse (with typical duration of 20 ns) if the pulse energy is large enough [32]–[34]. Extensive measurements on gratings made by this technique indicate a threshold-like phenomenon near a pulse energy level of about 35 mJ [34]. For lower pulse energies, the grating is relatively weak since index changes are only about 10^{-5} . By contrast, index changes of about 10^{-3} are possible for pulse energies above 40 mJ. Bragg gratings with nearly 100% reflectivity have been made by using a single 40-mJ

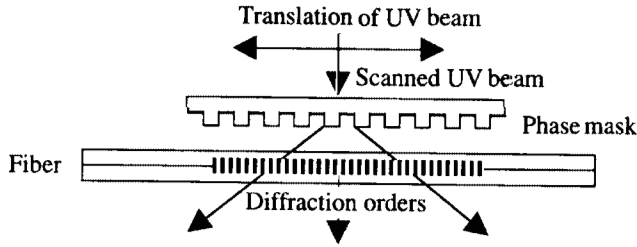


Figure 1.4: Schematic illustration of a phase-mask interferometer used for making fiber gratings. (After Ref. [48]; c 1999 Elsevier.)

pulse at the 248-nm wavelength. The gratings remained stable at temperatures as high as 800 C. A short exposure time has an added advantage. The typical rate at which a fiber is drawn from a preform is about 1 m/s. Since the fiber moves only 20 nm in 20 ns, and since this displacement is a small fraction of the grating period Λ , a grating can be written during the drawing stage while the fiber is being pulled and before it is sleeved [35]. This feature makes the single-pulse holographic technique quite useful from a practical standpoint.

1.2.3 Phase-Mask Technique

This nonholographic technique uses a photolithographic process commonly employed for fabrication of integrated electronic circuits. The basic idea is to use a phase mask with a periodicity related to the grating period [36]. The phase mask acts as a master grating that is transferred to the fiber using a suitable method. In one realization of this technique [37], the phase mask was made on a quartz substrate on which a patterned layer of chromium was deposited using electron-beam lithography in combination with reactive-ion etching. Phase variations induced in the 242-nm radiation passing through the phase mask translate into a periodic intensity pattern similar to that produced by the holographic technique. Photosensitivity of the fiber converts intensity variations into an index grating of the same periodicity as that of the phase mask.

The chief advantage of the phase-mask method is that the demands on the temporal and spatial coherence of the ultraviolet beam are much less stringent because of the noninterferometric nature of the technique. In fact, even a nonlaser source such as an ultraviolet lamp can be used. Furthermore, the phase-mask technique allows fabrication of fiber gratings with a variable period (chirped gratings) and can also be used to tailor the periodic index profile along the grating length. It is also possible to vary the Bragg wavelength over some range for a fixed mask periodicity by using a converging or diverging wavefront during the photolithographic process [41]. On the other hand, the quality of fiber grating (length, uniformity, etc.) depends completely on the master phase mask, and all imperfections are reproduced precisely. Nonetheless, gratings with 5-mm length and 94% reflectivity were made in 1993, showing the potential of this technique [37].

The phase mask can also be used to form an interferometer using the geometry shown in Figure 1.4. The ultraviolet laser beam falls normally on the phase mask and

is diffracted into several beams in the Raman–Nath scattering regime. The zeroth-order beam (direct transmission) is blocked or canceled by an appropriate technique. The two first-order diffracted beams interfere on the fiber surface and form a periodic intensity pattern. The grating period is exactly one-half of the phase-mask period. In effect, the phase mask produces both the reference and object beams required for holographic recording.

There are several advantages of using a phase-mask interferometer. It is insensitive to the lateral translation of the incident laser beam and tolerant of any beam-pointing instability. Relatively long fiber gratings can be made by moving two side mirrors while maintaining their mutual separation. In fact, the two mirrors can be replaced by a single silica block that reflects the two beams internally through total internal reflection, resulting in a compact and stable interferometer [48]. The length of the grating formed inside the fiber core is limited by the size and optical quality of the silica block.

Long gratings can be formed by scanning the phase mask or by translating the optical fiber itself such that different parts of the optical fiber are exposed to the two interfering beams. In this way, multiple short gratings are formed in succession in the same fiber. Any discontinuity or overlap between the two neighboring gratings, resulting from positional inaccuracies, leads to the so-called stitching errors (also called phase errors) that can affect the quality of the whole grating substantially if left uncontrolled. Nevertheless, this technique was used in 1993 to produce a 5-cm-long grating [42]. By 1996, gratings longer than 1 meter have been made with success [62] by employing techniques that minimize phase errors [63].

1.2.4 Point-by-Point Fabrication Technique

This nonholographic scanning technique bypasses the need of a master phase mask and fabricates the grating directly on the fiber, period by period, by exposing short sections of width w to a single high-energy pulse [19]. The fiber is translated by a distance $\Lambda - w$ before the next pulse arrives, resulting in a periodic index pattern such that only a fraction w/Λ in each period has a higher refractive index. The method is referred to as point-by-point fabrication since a grating is fabricated period by period even though the period Λ is typically below $1 \mu\text{m}$. The technique works by focusing the spot size of the ultraviolet laser beam so tightly that only a short section of width w is exposed to it. Typically, w is chosen to be $\Lambda/2$ although it could be a different fraction if so desired.

There are a few practical limitations of this technique. First, only short fiber gratings ($< 1 \text{ cm}$) are typically produced because of the time-consuming nature of the point-to-point fabrication method. Second, it is hard to control the movement of a translation stage accurately enough to make this scheme practical for long gratings. Third, it is not easy to focus the laser beam to a small spot size that is only a fraction of the grating period. Recall that the period of a first-order grating is about $0.5 \mu\text{m}$ at $1.55 \mu\text{m}$ and becomes even smaller at shorter wavelengths. For this reason, the technique was first demonstrated in 1993 by making a $360\text{-}\mu\text{m}$ -long, third-order grating with a $1.59\text{-}\mu\text{m}$ period [38]. The third-order grating still reflected about 70% of the incident $1.55\text{-}\mu\text{m}$ light. From a fundamental standpoint, an optical beam can be focused to a spot size as small as the wavelength. Thus, the 248-nm laser commonly

used in grating fabrication should be able to provide a first-order grating in the wavelength range from 1.3 to 1.6 μm with proper focusing optics similar to that used for fabrication of integrated circuits.

The point-by-point fabrication method is quite suitable for long-period gratings in which the grating period exceeds 10 μm and even can be longer than 100 μm , depending on the application [64]–[66]. Such gratings can be used for mode conversion (power transfer from one mode to another) or polarization conversion (power transfer between two orthogonally polarized modes). Their filtering characteristics have been used for flattening the gain profile of erbium-doped fiber amplifiers. Long-period gratings are covered in Section 1.7.1.

1.2.5 Technique based on Ultrashort Optical Pulses

In recent years, femtosecond pulses have been used to change the refractive index of glass locally and to fabricate planar waveguides within a bulk medium [67]–[72]. The same technique can also be used for making fiber gratings. Femtosecond pulses from a Ti:sapphire laser operating in the 800-nm regime were used as early as 1999 [73]–[75]. Two distinct mechanisms can lead to index changes when such lasers are used [76]. In the so-called type-I gratings, index changes are of reversible nature. In contrast, permanent index changes occur in type-II gratings because of multiphoton ionization and plasma formation when the peak power of pulses exceeds the self-focusing threshold. The second type of gratings can be written using energetic femtosecond pulses that illuminate an especially made phase mask [74]. They were observed to be stable at temperatures of up to 1000 C in the sense that the magnitude of index change created by the 800-nm femtosecond pulses remained unchanged over hundreds of hours [75].

In an alternative approach, infrared radiation is first converted into the UV region through harmonic generation, before using it for grating fabrication. In this case, photon energy exceeds 4 eV, and the absorption of single photons can create large index changes. As a result, the energy fluence required for forming the grating is reduced considerably [77]–[79]. In practice, one can employ either 264-nm pulses, obtained from fourth harmonic of a femtosecond Nd:glass laser, or 267-nm pulses using third harmonic of a Ti:sapphire laser. In both cases, index changes $>10^{-3}$ have been realized. Figure 1.5 shows the experimental results obtained when 264-nm pulses of 0.2-nJ energy (pulse width 260 fs) were employed for illuminating a phase mask and forming a 3-mm-long Bragg grating [77]. The left part shows the measured UV-induced change in the refractive index of fiber core as a function of incident energy fluence for (a) a hydrogen-soaked fiber and (b) a hydrogen-free fiber. The transmission spectra of three fiber gratings are also shown for fluence values that correspond to the maximum fluence level for the three peak intensities. The topmost spectrum implies a peak reflectivity level of $>99.9\%$ at the Bragg wavelength and corresponds to a UV-induced change in the refractive index of about 2×10^{-3} . This value was lower for the fiber that was not soaked in hydrogen, but it could be made to exceed 10^{-3} by increasing both the peak-intensity and fluence levels of UV pulses. Similar results were obtained when 267-nm pulses, obtained through third harmonic of a 800-nm Ti:sapphire laser, were employed [78]. Gratings formed with this method are of type-I type in the sense that the magnitude of index change decreases with annealing at high temperatures [79].

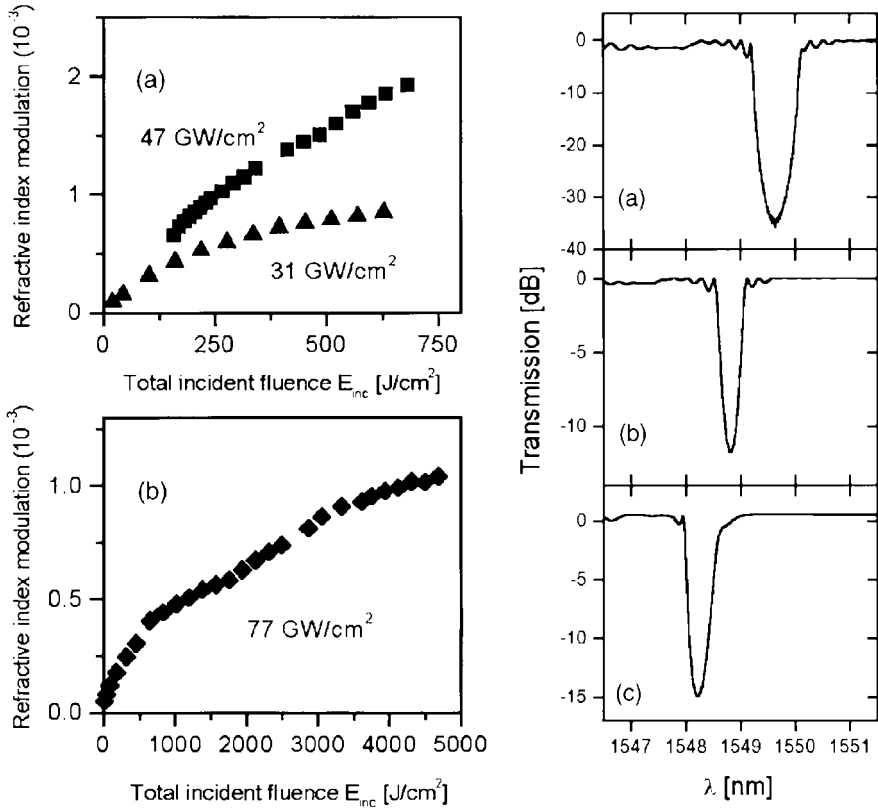


Figure 1.5: Left: Index change Δn as a function of incident energy fluence for (a) a hydrogen-soaked fiber and (b) a hydrogen-free fiber. Right: Transmission spectra of three fiber gratings for fluence values that correspond to the maximum fluence level at peak intensities of (a) $47 GW/cm^2$, (b) $31 GW/cm^2$, and (c) $77 GW/cm^2$. (After Ref. [77]; c 2003 OSA.)

1.3 Grating Characteristics

Two different approaches have been used to study how a Bragg grating affects wave propagation in optical fibers. In one approach, Bloch formalism—used commonly for describing motion of electrons in semiconductors—is applied to Bragg gratings [80]. In another, forward- and backward-propagating waves are treated independently, and the Bragg grating provides a coupling between them. This method is known as the *coupled-mode theory* and has been used with considerable success in several different contexts. In this section we derive the nonlinear coupled-mode equations and use them to discuss propagation of low-intensity CW light through a Bragg grating. We also introduce the concept of photonic bandgap and use it to show that a Bragg grating introduces a large amount of dispersion.

1.3.1 Coupled-Mode Equations

Wave propagation in a linear periodic medium has been studied extensively using coupled-mode theory [81]–[83]. This theory has been applied to distributed-feedback (DFB) semiconductor lasers [84], among other things. In the case of optical fibers, we need to include both the nonlinear nature and the periodic variation of the refractive index by using

$$\tilde{n}(\omega, z) = \bar{n}(\omega) + n_2|E|^2 + \delta n_g(z), \quad (1.3.1)$$

where n_2 is the nonlinear parameter and $\delta n_g(z)$ accounts for periodic index variations inside the grating. The coupled-mode theory can be generalized to include the fiber nonlinearity since the nonlinear index change $n_2|E|^2$ in Eq. (1.3.1) is so small that it can be treated as a perturbation [85].

The starting point consists of solving Maxwell's equations with the refractive index given in Eq. (1.3.1). However, as discussed in Section 2.3 of Ref. [2], if the nonlinear effects are relatively weak, we can work in the frequency domain and solve the Helmholtz equation

$$\nabla^2 \tilde{E} + \tilde{n}^2(\omega, z)\omega^2/c^2 \tilde{E} = 0, \quad (1.3.2)$$

where \tilde{E} denotes the Fourier transform of the electric field with respect to time.

Noting that \tilde{n} is a periodic function of z , it is useful to expand $\delta n_g(z)$ in a Fourier series as

$$\delta n_g(z) = \sum_{m=-\infty}^{\infty} \delta n_m \exp[2\pi im(z/\Lambda)]. \quad (1.3.3)$$

Since both the forward- and backward-propagating waves should be included, \tilde{E} in Eq. (1.3.2) is of the form

$$\tilde{E}(\mathbf{r}, \omega) = F(x, y)[\tilde{A}_f(z, \omega) \exp(i\beta_B z) + \tilde{A}_b(z, \omega) \exp(-i\beta_B z)], \quad (1.3.4)$$

where $\beta_B = \pi/\Lambda$ is the Bragg wave number for a first-order grating. It is related to the Bragg wavelength through the Bragg condition $\lambda_B = 2\bar{n}\Lambda$ and can be used to define the Bragg frequency as $\omega_B = \pi c/(\bar{n}\Lambda)$. Transverse variations for the two counterpropagating waves are governed by the same modal distribution $F(x, y)$ in a single-mode fiber.

Using Eqs. (1.3.1)–(1.3.4), assuming \tilde{A}_f and \tilde{A}_b vary slowly with z , and keeping only the nearly phase-matched terms, the frequency-domain coupled-mode equations become [81]–[83]

$$\frac{\partial \tilde{A}_f}{\partial z} = i[\delta(\omega) + \Delta\beta]\tilde{A}_f + i\kappa\tilde{A}_b, \quad (1.3.5)$$

$$\frac{\partial \tilde{A}_b}{\partial z} = i[\delta(\omega) + \Delta\beta]\tilde{A}_b + i\kappa\tilde{A}_f, \quad (1.3.6)$$

where δ is a measure of detuning from the Bragg frequency and is defined as

$$\delta(\omega) = (\bar{n}/c)(\omega - \omega_B) - \beta(\omega) - \beta_B. \quad (1.3.7)$$

The nonlinear effects in the coupled-mode equations are included through $\Delta\beta$. The coupling coefficient κ governs the grating-induced coupling between the forward and backward waves. For a first-order grating, κ is given by

$$\kappa = \frac{k_0 \iint_{-\infty}^{\infty} \delta n_1 |F(x, y)|^2 dx dy}{\iint_{-\infty}^{\infty} |F(x, y)|^2 dx dy}. \quad (1.3.8)$$

In this general form, κ can include transverse variations of δn_g occurring when the photoinduced index change is not uniform over the core area. For a transversely uniform grating $\kappa = 2\pi\delta n_1/\lambda$, as can be inferred from Eq. (1.3.8) by taking δn_1 as constant and using $k_0 = 2\pi/\lambda$. For a sinusoidal grating of the form $\delta n_g = n_a \cos(2\pi z/\Lambda)$, $\delta n_1 = n_a/2$ and the coupling coefficient is given by $\kappa = \pi n_a/\lambda$.

Equations (1.3.5) and (1.3.6) can be converted to time domain by following the procedure outlined in Section 2.3 of Ref. [2]. We assume that the total electric field can be written as

$$E(\mathbf{r}, t) = \frac{1}{2} F(x, y) [A_f(z, t) e^{i\beta_B z} + A_b(z, t) e^{-i\beta_B z}] e^{i\omega_0 t} + \text{c.c.}, \quad (1.3.9)$$

where ω_0 is the frequency at which the pulse spectrum is centered. We expand $\beta(\omega)$ in Eq. (1.3.7) in a Taylor series as

$$\beta(\omega) = \beta_0 + (\omega - \omega_0)\beta_1 + \frac{1}{2}(\omega - \omega_0)^2\beta_2 + \frac{1}{6}(\omega - \omega_0)^3\beta_3 + \quad (1.3.10)$$

and retain terms up to second order in $\omega - \omega_0$. The resulting equations are converted into the time domain by replacing $\omega - \omega_0$ with the differential operator $i(\partial/\partial t)$. The resulting time-domain coupled-mode equations have the form

$$\frac{\partial A_f}{\partial z} + \beta_1 \frac{\partial A_f}{\partial t} + \frac{i\beta_2}{2} \frac{\partial^2 A_f}{\partial t^2} + \frac{\alpha}{2} A_f = i\delta A_f + i\kappa A_b + i\gamma(|A_f|^2 + 2|A_b|^2)A_f, \quad (1.3.11)$$

$$\frac{\partial A_b}{\partial z} + \beta_1 \frac{\partial A_b}{\partial t} + \frac{i\beta_2}{2} \frac{\partial^2 A_b}{\partial t^2} + \frac{\alpha}{2} A_b = i\delta A_b + i\kappa A_f + i\gamma(|A_b|^2 + 2|A_f|^2)A_b, \quad (1.3.12)$$

where δ in Eq. (1.3.7) is evaluated at $\omega = \omega_0$ and becomes $\delta = (\omega_0 - \omega_B)/v_g$. In fact, the δ term can be eliminated from the coupled-mode equations if ω_0 is replaced by ω_B in Eq. (1.3.9). The other parameters have their traditional meaning. Specifically, $\beta_1 = 1/v_g$ is related inversely to the group velocity, β_2 governs the group-velocity dispersion (GVD), and the nonlinear parameter γ is related to n_2 as $\gamma = n_2\omega_0/(cA_{\text{eff}})$, where A_{eff} is the effective mode area (see Ref. [2]).

The nonlinear terms in the time-domain coupled-mode equations contain the contributions of both self-phase modulation (SPM) and cross-phase modulation (XPM). In fact, the coupled-mode equations are similar to and should be compared with Eqs. (7.1.15) and (7.1.16) of Ref. [2], which govern the propagation of two copropagating waves inside optical fibers. The two major differences are: (i) the negative sign appearing in front of the $\partial A_b/\partial z$ term in Eq. (1.3.11) because of backward propagation of A_b and (ii) the presence of linear coupling between the counterpropagating waves governed by the parameter κ . Both of these differences change the character of wave propagation profoundly. Before discussing the general case, it is instructive to consider the case in which the nonlinear effects are so weak that the fiber acts as a linear medium.